PCCP

Accepted Manuscript

ROYAL SOCIETY OF CHEMISTRY

www.rsc.org/pccp

Journal Name

ARTICLE

Hybrid functional study of the NASICON-type $Na_3V_2(PO_4)_3$: Crystal and electronic structures, and polaron-Na vacancy complex diffusion

Received 00th January 20xx,
Accepted 00th January 20xx

DOI: 10.1039/x0xx00000x

www.rsc.org/

Kieu My Bui,[a,b] Van An Dinh,[c] Susumu Okada,[b] and Takahisa Ohno[a,d,e]

The crystal and electronic structures, electrochemical properties, and diffusion mechanism of the NASICON-type $Na_3V_2(PO_4)_3$ are investigated based on the hybrid density functional Heyd-Scuseria-Ernzerhof (HSE06). The polaron-Na vacancy complex model for revealing the diffusion mechanism is proposed for the first time in Na ion battery field. The bound polaron is found to favorably form at the first nearest V site to the Na vacancy. Consequently, the movement of the Na vacancy will be accompanied by the polaron. Three preferable diffusion pathways are revealed; those are two intra-layer diffusion pathways and one inter-layer pathway. The activation barriers for the intra-layer and inter-layer pathways are 353 meV and 513 meV, respectively. For further comparison, the generalized gradient approximation with an onsite Coulomb Hubbard U (GGA+U) is also employed.

1. Introduction

Electrical energy storage (EES) has made irreplaceable contribution to the world's energy supplies, especially since the important issues such as the raising of global warming, the running out of non-renewable energy sources, and the increasing of human demand for energy have become dramatic.[1] Among various electrical energy storages, rechargeable batteries are now dominating the market due to their compact size, high performance, and environmentally-friendliness. Owing to high volumetric and gravimetric energy densities, lithium-ion batteries (LIBs) are now growing rapidly and becoming more and more effective.[2,3] Indeed, LIBs have wide range of application from small to large power devices.[4] Especially in the energy storage market for portable devices, LIBs are keeping a premier position. However, for large-scale applications where the most important factor is the cost and abundance instead of energy density, sodium-ion batteries (SIBs) seem to be more suitable than LIBs.[5-8] Na is not only the sixth most abundant element on earth crust but also a very cheap material (Price for Li carbonate: 4.11–4.49 €/kg, Na carbonate: 0.07–0.37 €/kg).[6] The diffusion of Na in SIBs can also be comparable to that of Li in LIBs.[9] Hence, extensive research about SIBs should be carried out because of such merits. Furthermore, we can also take advantage of the previous studies on LIBs since the chemical natures of Li and Na are similar. However, the heavier weight and larger ionic radius of Na (m_{Na} = 23 g/mol, r_{Na} = 0.98 Å) compared to Li (m_{Li} = 6.9 g/mol, r_{Li} = 0.69 Å)[6] make it harder to intercalate/deintercalate Na than Li, hence reduce the performance of the materials. Therefore, it is needed to find electrode materials where Na atoms can be easily intercalated/deintercalated.

Lately, many cathode materials such as the layered structure (Na_xMO_2, M= V, Cr, Mn, Co),[10,11] the olivine and maricite structures ($NaFePO_4$, $NaV_{1-x}Cr_xPO_4F$),[12,13] and the NASICON-type materials ($Na_3M_2(PO_4)_3$ (M = Ti, Fe, and V) and $Na_3V_2(PO_4)_3F$)[14-16] have been widely studied. Among them, the vanadium-based NASICON material, namely $Na_3V_2(PO_4)_3$ [17-28] (NVP) whose structure is built of three dimension $V_2(PO_4)_3$ framework, is attracting attention as a promising cathode material. The name of NASICON is the acronym for sodium (Na) Super Ionic CONductor which comes from the family $Na_{1+x}Zr_2Si_xP_{3-x}O_{12}$ (0<x<3).[29] The NASICON structure, which is famous for its high ionic conductivity, provides large ionic sites in which lithium or sodium atoms can be inserted, hence it can be used for both LIBs and SIBs.[30,31] It was proved that $Na_3V_2(PO_4)_3$ can be reversibly intercalated/deintercalated. For this reason, the material is considered as a multifunctional electrode which is able to be used as not only cathode but also anode. $Na_3V_2(PO_4)_3$ shows two voltage plateau at 3.4 V and 1.6 V, which may correspond to V^{4+}/V^{3+} and V^{3+}/V^{2+} redox couples.[19,20] More recently, NVP has been fabricated as cathode/anode for the all-solid state NASICON sodium batteries with NVP/electrolyte/NVP structures.[32,33] To the best of our knowledge, there is no systematic study on the Na diffusion in NVP in the literature.

Previously, it was proved that as a Li vacancy is introduced in $LiMPO_4$ (M = Fe, Mn),[34-37] Li_2MSiO_4 (M = Fe, Mn, Ni),[38-40] and $Li_3FePO_4CO_3$,[41] a small polaron would form at a transition metal site. Dinh *et. al.*[37] suggested a polaron-Li vacancy complex model in which the Li diffusion should be accompanied with the migration of the polaron. Later on, Bui *et. al.*[38-40] and Duong *et. al.*[41] successfully applied the model on Li_2MSiO_4 and $Li_3FePO_4CO_3$, respectively. According to their calculations, the GGA+U method was proved to be an appropriate method to deal well with the diffusion problem

[a] Global Research Center for Environment and Energy based on Nanomaterials Science (GREEN), Namiki 1-1, Tsukuba, Ibaraki 305-0044, Japan. Email: BUI.Thikieumy@nims.go.jp
[b] Graduate School of Pure and Applied Sciences, University of Tsukuba, 1-1-1 Tennodai, Tsukuba, Ibaraki 305-8577, Japan. Email: sokada@comas.frsc.tsukuba.ac.jp
[c] Graduate School of Engineering, Osaka University. Yamadaoka 2-1, Suita, Osaka 565-0871, Japan. Email: divan@mat.eng.osaka-u.ac.jp
[d] Computational Materials Science Unit (CMSU), National Institute for Materials Science (NIMS), Sengen 1-2-1, Tsukuba, Ibaraki 305-0047, Japan. Email: OHNO.Takahisa@nims.go.jp
[e] Institute of Industrial Science, University of Tokyo, Meguro, Tokyo 153-8505, Japan.

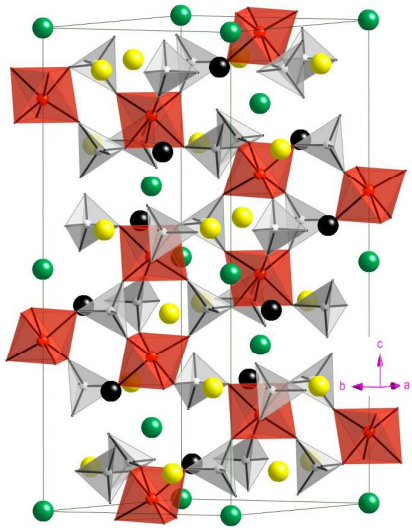

Fig. 1 The crystal structure of NVP. Na at the Na_1 site are shown by dark green balls, Na at the Na_2 site by yellow balls, and the empty Na sites by black balls. The V octahedra are shown by red and the P tetrahedra by grey.

in $LiFePO_4$, $Li_3FePO_4CO_3$, and Li_2FeSiO_4 systems. Nevertheless, in $LiMnPO_4$, Li_2MnSiO_4 and Li_2NiSiO_4, the hybrid density functional HSE06 method is found to be more appropriate in addressing the polaron localization in the material. Since the Hubbard U parameter in the GGA+U method was designed to treat only the electron correlation in d states of transition metal oxides, this method may not be appropriate in the system where d states are not well localized. Fortunately, the hybrid functional could handle the polaron problem well, albeit it is a time consumer. The benefit of the hybrid functional is that it incorporates the exact Hartree-Fock (HF) and density functional theory (DFT) to generate an exact exchange mixing, hence performs a more universal treatment. For this reason, the time-consuming HSE06 method was used.

2. Method of calculations

The new PBE0 hybrid functional that approximates the exchange correlation by incorporating a certain amount of the exact exchange HF with DFT is used. It has the form:

$$E_{xc}^{\mathrm{PBE0}} = aE_x^{\mathrm{HF}} + (1-a)E_x^{\mathrm{PBE}} + E_c^{\mathrm{PBE}}$$

By eliminating the compensated HF and PBE long-range exchange contribution, the following form is obtained:

$$E_{xc}^{\omega\mathrm{PBEh}} = aE_x^{\mathrm{HF,SR}}(\omega) + (1-a)E_x^{\mathrm{PBE,SR}}(\omega) + E_x^{\mathrm{PBE,LR}}(\omega) + E_c^{\mathrm{PBE}}$$

where a is mixing coefficient and ω is an adjustable parameter handling the short-range interactions extension. HSE06[42] is the hybrid functional version that employs $a = 1/4$ and $\omega = 0.2$. This method has already been proved to be reliable to deal well with many systems.

Here, we report about the application of the polaron-Li vacancy complex model on the NASICON-type NVP using the HSE06 method. For comparison, the result of GGA+U[43] where U_{eff} = 4.2 eV is presented. Both bulk and geometry with one vacancy were fully optimized. The convergence condition of the residual force was set at 10^{-2} eV/Å. Then, we defined the Na diffusion pathways by addressing the elementary diffusion processes and calculated the corresponding activation barriers using the nudged elastic band (NEB)[44] method. All the calculations presented here were carried out using the Vienna ab initio simulation package (VASP).[45] The space group of NVP is rhombohedral $R\bar{3}c$ which contains of six formula units (f.u.). In this research, the calculations were carried out for the primitive cell containing two f.u.. For the GGA+U calculation, a 4×4×4 *k*-point grid was used. Because of the time-consuming HSE method, we used the Γ-centered 2×2×2 *k*-point grid for the HSE06 calculation. The cut-off energy was set at 500 eV for generating the plane wave basis set.

Table 1. The calculated and experimental lattice parameters (Å) in $Na_3V_2(PO_4)_3$ and $Na_1V_2(PO_4)_3$.

	a,b (Å)	c (Å)
$Na_3V_2(PO_4)_3$	8.682 (Experiment[15]) 8.719 (HSE06) 8.826 (GGA+U)	21.712 21.422 21.634
$Na_1V_2(PO_4)_3$	8.427 (HSE06), 8.557 (GGA+U)	21.403 21.529

Table 2. The bond distances (Å) of Na_1-O, Na_2-O, P-O, and V-O in $Na_3V_2(PO_4)_3$ and $Na_1V_2(PO_4)_3$. The experimental values are extracted from the suggested experimental geometrical structure.[15]

	$Na_3V_2(PO_4)_3$			$Na_1V_2(PO_4)_3$	
	Experiment[15]	Calculation		Calculation	
		HSE06	GGA+U	HSE06	GGA+U
Na_1-O (Å)	6×2.40	2×2.38 2×2.39 2×2.47	2×2.40 2×2.41 2×2.49	2×2.42 2×2.43 2×2.49	2×2.49 2×2.50 2×2.51
Na_2-O (Å)	2×2.39 2×2.43 2×2.59	2×2.39 2×2.41 2×2.49	2×2.41 2×2.43 2×2.52		
P-O (Å)	2×1.53 2×1.57	2×1.53 2×1.55	2×1.54 2×1.56	1.52 1.52 1.53 1.56	1.55 1.56 1.56 1.57
V-O (Å)	3×1.94 3×2.04	3×1.94 3×2.04	3×1.99 3×2.07	1.82 1.88 1.90 1.91 1.96 1.96	1.88 1.90 1.91 1.96 1.97 1.97

3. Results and discussion

NVP possesses the rhombohedral NASICON structure as shown in Fig. 1. NASICON structure is a three-dimensional framework built of $[V_2(PO_4)_3]$ units created by corner-sharing of octahedra VO_6 and tetrahedra PO_4 along *c*-axis direction. Accordingly, the hexagonal bottlenecks are formed by corner-sharing of three octahedra VO_6 and three tetrahedra PO_4. The shortest diameter of the bottleneck is as large as 4.74 Å, which approximately equals to twice the sum of the Na^+ and O^{2-} ionic radii. During diffusion, these hexagonal

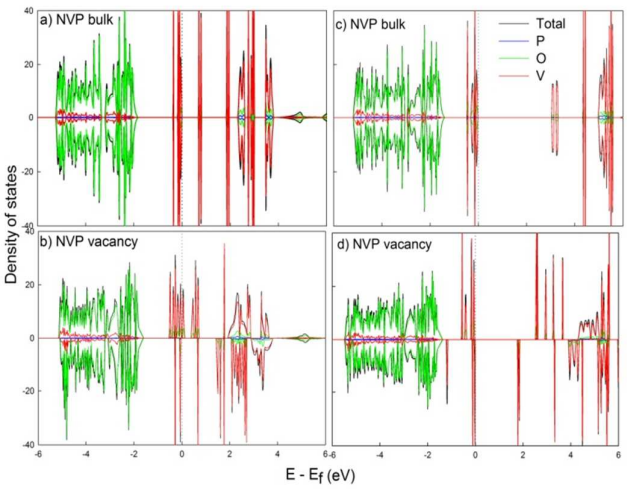

Fig. 2 The antiferromagnetic density of states for the bulk and vacancy of NVP obtained by (a,b) GGA+U and (c,d) HSE06 methods.

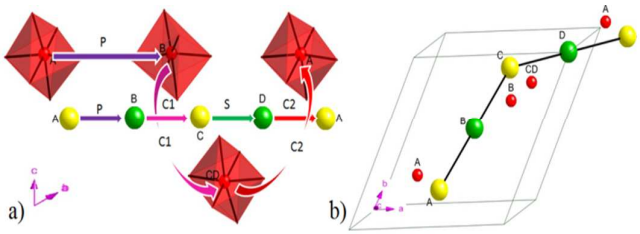

Fig. 3 Schematic of Pathway 1. (a) Polyhedral model. The purple, pink, green and red arrows represent the path of the P, C_1, S and C_2 processes, respectively. (b) Ball and stick model in the *c*-direction view.

bottlenecks provide large interstitial sites in which Na can easily diffuse. There are two different types of Na sites in a formula unit of $Na_4V_2(PO_4)_3$: one Na_1 site locates in an $[V_2(PO_4)_3]$ unit along the *c*-direction, and three Na_2 sites have the same *c*-coordinates with adjacent P atoms. A f.u. of NVP includes one Na occupying the Na_1 site and two Na occupying the Na_2 sites. Our calculation shows that the energy difference between the structures with a vacancy at Na_1 site or at Na_2 site is $\Delta E = E_{Na1} - E_{Na2} = 75$ meV. Hence, Na at the Na_2 site is likely to be more mobile than that at Na_1. This is in accordance with the previous study[31] which reported that in NVP, the occupancy of the Na_1 site is 1.0 while that of the Na_2 site is 0.67. Besides, the other occupancy possibility of Na at Na_1 site and Na_2 site is reported by Song *et. al.*.[28] The geometrical parameters obtained by the HSE06 (GGA+U) method are $a = b = 8.719$ (8.826) Å, $c = 21.422$ (21.634) Å. As shown in Table 1, the results obtained by HSE06 and GGA+U are in good agreement with the experimental data. Our calculations show that the Na deintercalation will cause a slight contraction of lattice parameters along the *a* and *c* axes as shown in Table 1. All calculations in this research are spin-polarized antiferromagnetic (AFM) since the magnetic ground state of the material is AFM. Ferromagnetic arrangement (FM) is nearly as stable as AFM ($\Delta E = E_{FM} - E_{AFM} = 8$ meV/f.u.) while nonmagnetic one (NM) is the most unstable state ($\Delta E = E_{NM} - E_{AFM} = 2.4$ eV/f.u.). The results of the bond distances between cations (Na, P and V) and oxygen ions in $Na_3V_2(PO_4)_3$ and $Na_1V_2(PO_4)_3$ are summarized in Table 2. Referring to this table, we found that for NVP, HSE06 and

Table 3. V*i* – O*j* (*i* = 1-4, *j* = 1-6) indicates the bond distance (Å) in the NVP with one vacancy. The V atoms indexed by *i* = 1, 3, 4 are with +3 oxidation; *i* = 2 is with +4 oxidation. The parameters are calculated by the HSE06 (GGA+U) method.

V*i* – O*j* (Å)	Average	*j* = 1	*j* = 2	*j* = 3	*j* = 4	*j* = 5	*j* = 6
i = 1	1.99 (2.00)	1.94 (1.92)	1.97 (1.98)	1.97 (2.01)	1.97 (2.00)	2.03 (2.04)	2.03 (2.07)
i = 2	1.92 (2.00)	1.81 (1.91)	1.91 (1.96)	2.00 (2.04)	1.91 (2.01)	1.93 (2.03)	1.98 (2.07)
i = 3	2.00 (2.03)	1.93 (1.96)	1.93 (1.96)	2.00 (2.01)	2.00 (2.05)	2.02 (2.06)	2.09 (2.14)
i = 4	2.02 (2.03)	1.93 (1.92)	1.97 (1.98)	2.05 (2.03)	2.02 (2.05)	2.06 (2.09)	2.10 (2.12)

Table 4. Distances (Å) from Na_1 and Na_2 sites to the nearest V sites in the bulk of NVP. Results are obtained by the HSE06 (GGA+U) method.

Site	1NN	2NN	3NN	4NN
Na_1	3.214 3.154	3.214 3.154	4.963 5.089	4.963 5.089
Na_2	3.077 3.095	3.140 3.159	3.877 3.943	3.897 3.962

GGA+U give similar bond lengths to the experiment. The Na_1 site and Na_2 site have different oxygen surrounding environments. P-O bonds remain almost constant during Na moves. This may help NVP to maintain its stability during intercalation/deintercalation. HSE06 (GGA+U) calculation shows that average V-O bonds decrease from 1.99 Å (2.03 Å) to 1.91 Å (1.93 Å) during deintercalation. Such a bond-length shrinkage is due to the change of the oxidation state of V from V^{3+} in $Na_3V_2(PO_4)_3$ to V^{4+} in $Na_1V_2(PO_4)_3$.

There are many first-principles studies have shown that the deintercalation/intercalation voltage in various Li-based as well as Na-based compounds[9,46] can be approximated by the following equation:

$$V = -\frac{E(\mathrm{A}_n\mathrm{H}) - E(\mathrm{A}_{n-x}\mathrm{H}) - xE(\mathrm{A})}{xe}$$

where E is the total energy, A is alkali atom, $\mathrm{A}_n\mathrm{H}$ is the host structure, x is the number of alkali transferred, and e is the absolute value of the electron charge. By using the above formula, the calculated voltage obtained by HSE06 is 3.30 V which is in good agreement with the experimental result of 3.40 V.[20] On the other hand, the voltage of 2.51 V obtained by GGA+U is smaller than the experimental value.

Fig. 2 illustrates the spin-polarized density of state (DOS) of the bulk NVP and the defect NVP. The projected DOS calculated by GGA+U and HSE06 of the 3*d*-state of V atoms and the 2*p*-state of P and O atoms are also presented. As seen from the projected DOS, the states at low energy regions are mainly contributed by 2*p*-states of O atoms while those at high energy regions are dominated by 3*d*-states of V atoms. The HSE06 method gives a larger band gap ($Eg_{HSE06} = 3.25$eV) than GGA+U ($Eg_{GGA+U} = 0.77$eV). As of such band gap range, the material can be considered as a semiconductor. When a Na vacancy is introduced in the material, one of the V atoms would change its oxidation state from V^{3+} to V^{4+}, resulting in

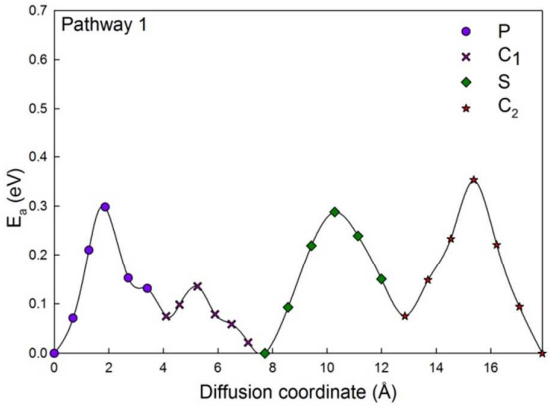

Fig. 4 Activation energies of the polaron-Na vacancy diffusion in NVP along Pathway 1. The purple circles, pink crosses, green diamonds and red stars represent the activation energy profile of the P, C_1, S and C_2 elementary diffusion processes, respectively.

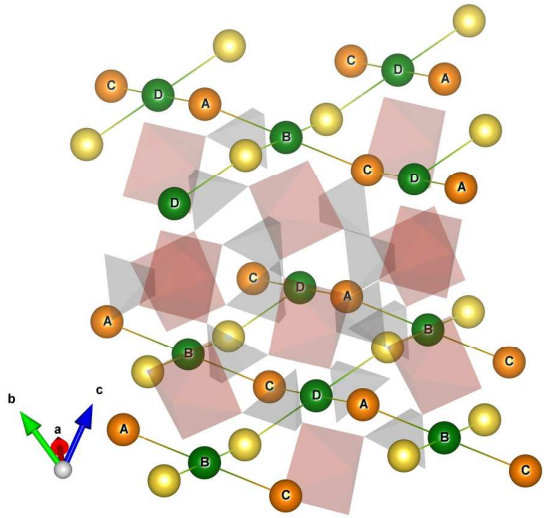

Fig. 5 Schematic of Pathway 1 and 2. The orange-green lines that connect orange Na balls and green Na balls represent for Pathway 1, and the yellow-green lines that connect yellow Na balls and green Na balls represent for Pathway 2.

the formation of a small polaron. In DOS of GGA+U, the spin-polarized picture appears but it is hard to recognize if the bound states form in the band gap. For the NVP bulk, both methods generate the same local magnetic moment of V^{3+} (1.92 μ_B). The fact of the calculated local magnetic moment of a V ion near the Na vacancy changes to 1.04 μ_B in HSE06 calculation implies that V ion at that site changes its oxidation to +4. On the contrary, the local magnetic moment of 1.64 μ_B by GGA+U suggests that GGA+U fails for this case. The V-O bond length in NVP with defect is given in Table 3. The shrinkage of V-O bonds when the oxidation state of V changed from +3 to +4 was not observed in GGA+U calculation. The charge in GGA+U is not well localized, hence the formation of polaron at V site is not well described. The HSE06 results show two important evidences for the presence of the polaron: the appearance of the bound states and the lattice distortions. We can see the bound states in the band-gap in DOS of the defect NVP. As

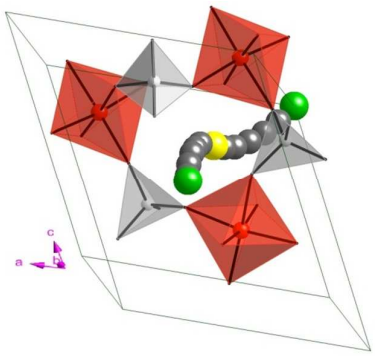

Fig. 6 Diffusion route through hexagonal bottlenecks. The deep grey ball is the transition Na.

seen from Table 3, the V-O bonds contract from 2.00 Å to 1.92 Å as a consequence of the change in the oxidation state of V from V^{3+} to V^{4+}. In short, the HSE06 functional is suitable to deal with polaron formation localization, whereas GGA+U is unfulfilled in describing the polaron formation in this material. Therefore, it is necessary to use the time-consuming HSE06 to deal with polaron problem in this material.

Table 4 demonstrates distances from the Na-sites to its four nearest V sites. The Na_1 site and Na_2 site have different V surrounded environments. The bound polaron is found to favorably form at the first nearest V site.

As a Na vacancy diffuses, a polaron would simultaneously migrate with the Na vacancy. Therefore, the Na diffusion should be treated as diffusion of the polaron-Na vacancy complex.[37] From the previous studies, it can be seen that depending on the system, the diffusion of the polaron-Li vacancy complex[37,38,41] can process in one-, two- or quasi-three dimensions. In NVP, the polaron-Na vacancy diffusion is in three dimensions as described below.

In NVP, three different diffusion pathways are available: two intra-layer pathways (Pathway 1 and Pathway 2) and one inter-layer pathway (Pathway 3). First, we reveal the diffusion along pathways inside of a Na layer. Let us index the sites where the Na vacancy passes through along Pathway 1 as *I* (*I*= A, B, C, and D). The site of the bound polaron accompanied with the Na vacancy at *I*-site is indexed by V_I. Because Na vacancies at C and D are accompanied with the same polaron, the site of this polaron will be indexed as V_{CD}. Thus, when the Na vacancy goes through the *I* site, the accompanied polaron will migrate through the V_I site. There are four elementary processes in Pathway 1, this is, two crossing processes C_1 and C_2, one parallel process P and one single diffusion process S as described in Fig. 3. Here, the term "parallel" indicates that the moving direction of the Na vacancy and that of its accompanied polaron are parallel as shown in Fig. 3a, while the term "crossing" indicates the opposite situation. Furthermore, the process in which the polaron stays on the same site during the Na vacancy diffuses is called as a single process. The Na vacancy moves along the *b*-direction in processes P and C_1, and along the *a*-direction in processes S and C_2, as illustrated in Fig. 3b. Elementary process P is the process in which the Na vacancy moves from A to B, while its polaron migrates from V_A to V_B. Process C_1 describes the motion of the Na vacancy from B to C, and the accompanied migration of its polaron from V_B to V_{CD}. In S process, when the Na vacancy diffuses from C to D, there is no polaron hopping since the Na vacancies at C and D have the same accompanied polaron. C_2 describes the diffusion process of the Na vacancy from D to A, while

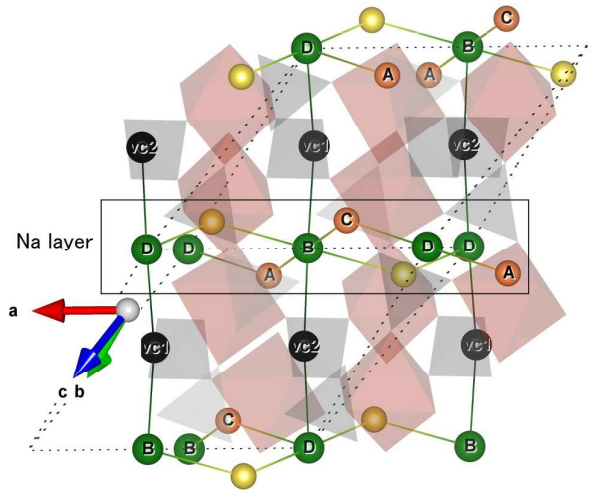

Fig. 7 Schematic of Pathway 1, 2 and 3. The black-green lines that connect Na at the Na_1 site and the Na vacancy represent for Pathway 3.

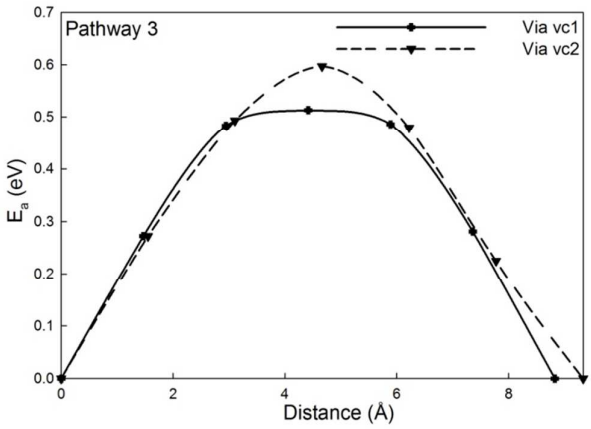

Fig. 8 Activation energies of the polaron-Na vacancy diffusion in NVP along Pathway 3. The solid curve represents for the diffusion process through vc1 while the dash curves represents for that through vc2.

its polaron from V_{CD} to V_A. If the Na vacancy forms at the Na_2 site (say A, C), there is no severe change in the surrounding environment. On the contrary, the vacancy at the Na_1 site, (say B) would attract Na at C to come closer and also give rise to some slight change in the location of the other Na ions in the cell. Therefore, the diffusion distance of the path connecting B with C, *i.e* process C_1, is as small as 2.5 Å, leading to the very low activation barrier of 137 meV. The activation barriers for P, S and C_2 processes are 283, 288 and 353 meV, respectively. The overall activation barrier for this pathway is 353 meV, as described in Fig. 4.

The diffusion mechanism and activation barrier of the polaron-Na vacancy complex in Pathway 2 is similar to that in Pathway 1. While Pathway 1 proceeds in the (112) plane, Pathway 2 crosses Pathway 1 and takes place in the (121) plane as described in Fig. 5. Fig. 6 depicts the trajectory of the diffusion in Pathway 1 and 2. As we described before in the structural properties part, the Na vacancy has to diffuse through the hexagonal bottleneck of VO_6 octahedra and PO_4 tetrahedra in every elementary process. Furthermore, the diffusion in Pathway 1 and 2 always take place from the Na_1 site to the Na_2 site and move along parabolic-liked trajectory. Besides, we also investigate the route in which Na does not move through the hexagonal bottleneck. In this case, it is the direct Na_2 site to Na_2 site diffusion, particularly from A (or C) to their nearest Na_2 site neighbor. Since there is no large enough space for Na to diffuse, Na has to climb an energy barrier of 1.2 eV. Because of such high barrier, this route is not a preferable pathway. Consequently, the diffusion of Na inside of a Na layer preferably happens along Pathway 1 and Pathway 2.

Next, we investigate the diffusion between two adjacent Na layers. Pathway 3 shown in Fig. 7 is one of that called the inter-layer pathways because it connects the Na layers. In $Na_3V_2(PO_4)_3$ structure, there are two empty Na sites, named as vc_1 and vc_2. These empty sites lie in the space between two adjacent Na layers, which Na could pass through during diffusion from a Na layer to its adjacent layer as shown in Fig. 7. To reveal which diffusion path is the most preferred, we do the NEB calculation by choosing B and D as an initial and final position of the Na vacancy and create replicates (intermediate images) using the linear interpolation. There are two ways along which the diffusion may take place: one passes through vc_1 and the other through vc_2. According to Fig. 8, the calculated activation energy of the diffusion processes via vc_1 and vc_2 are 513 meV and 597 meV, respectively. This means that the Na vacancy may prefer to diffuse through layers via vc_1. Similar to the diffusion in Pathways 1 and 2, the Na in Pathway 3 also passes through the hexagonal bottleneck. In addition to Pathway 3, the possibility of diffusion along the other inter-layer trajectories that does not proceed through the hexagonal bottleneck, such as the route connecting two Na ions at the Na_2 sites, is also considered. The diffusion in that route encounters a very high barrier of 3 eV, hence Na preferably moves along Pathway 3 when it jumps to the adjacent layers.

Conclusions

In summary, the density functional theory with the HSE06 and GGA+U methods was utilized to predict the geometrical as well as the electronic structure, the intercalation/deintercalation voltages and the Na diffusion mechanism in NVP. The results of the structures and average voltages in these methods are in good agreement with the previous experimental data. The material is semiconductor. Similar to the $LiMnPO_4$, Li_2MnSiO_4, and Li_2NiSiO_4 cases, the GGA+U is unfulfilled in handling the polaron problem in NVP. On the other hand, HSE06 was proved to be an effective tool to manage the polaron localization. As a Na vacancy is introduced, the polaron would form at the first nearest neighbour V site to the Na vacancy. Diffusion of Na ions was treated as a process of the polaron-Na vacancy complexes. Diffusion processes inside of a Na layer and between the adjacent layers were investigated. Two intra-layer pathways and one inter-layer pathway were explored and the activation energy profiles were calculated. The activation barrier of the intra-layer diffusion is 353 meV, while that of the inter-layer diffusion gains a significantly higher value of 513 meV, respectively. Because of the lower barrier of Pathway 1, as well as Pathway 2, compared with that of Pathway 3, the diffusion of Na inside Na layers is easier than between layers. In preferable pathways, Na always diffuses through the large space of hexagonal bottleneck.

Acknowledgments

This work was supported by the MEXT Program for Development of Environment Technology using Nanotechnology. K.M.Bui is grateful to Dr. M. Khazaei for the valuable discussion.

Notes and references

1 B. Dunn, H. Kamath and J. -M. Tarascon, *Science*, 2011, **334**, 928.
2 J. -M. Tarascon and M. Armand, *Nature,* 2001, **414**, 359.
3 J. B. Goodenough and K. S. Park, *J. Am. Chem. Soc.*, 2013, **135** (4), 1167.
4 J. Pistoia, *Lithium-Ion Batteries: Advances and Applications*, Elsvier 2014.
5 N. Yabuuchi, K. Kubota, M. Dahbi and S. Komaba, *Chem. Rev.*, 2014, **114**, 11636.
6 V. Palomares, P. Serras, I. Villaluenga, K. B. Hueso, J. C. Gonzalez and T. Rojo, *Energy Environ. Sci.,* 2012, **5**, 5884.
7 B. L. Ellis and L. F. Nazar, *Curr. Opin. Solid State Mater. Sci.*, 2012, **16**, 168.
8 M. D. Slater, D. Kim, E. Lee and C. S. Johnson, *Adv. Funct. Mater.,* 2013, **23**, 947.
9 S. P. Ong, V. L. Chevrier, G. F. Hautier, A. Jain, C. Moore, S. Kim, X. Ma and G. Ceder, *Energy Environ. Sci.*, 2011,**4**, 3680.
10 J. J. Ding, Y. N. Zhou, Q. Sun and Z. W. Fu, *Electrochem.Commun.*, 2012, **22**, 85.
11 R. Berthelot, D. Carlier and C. Delmas**,** *Nature Materials,* 2011, **10**, 74.
12 S. M. Oh, S. T. Myung, J. Hassoun, B. Scrosat and Y. K. Sun, *Electrochem. Commun.,* 2012, **14**, 149.
13 H. T. Zhuo, X. Y. Wang, A. P. Tang, Z. M. Liu, S. Gamboa and P. J. Sebastian, *J. Power Sources,* 2006, **160**, 698.
14 H. Kabbour, D. Coillot, M. Colmont, C. Masquelier and O. Mentre, *J. Am. Chem. Soc.*, 2011, 133, 11900.
15 J. Gopalakrishnan and K.K. Rangan, *Chem. Mater.*, 1992, **4**, 745.
16 W. Song, X. Cao, Z. Wu, J. Chen, Y. Zhu, H. Hou, Q. Lan and X. Ji, *Langmuir*, 2014, **30(41)**, 12438.17 K. Du, H. Guo, G. Hu, Z. Peng and Y. Cao, *J. Power Sources*, 2013, **223**, 284.
18 M. Pivko, I. Arcon, M. Bele, R. Dominko and M. Gaberscek, *J. Power Sources*, 2012, **216**, 145.
19 J. Kang, S. Baek, V. Mathew, J. Gim, J. Song, H. Park, E. Chae, A. K. Rai and J. Kim, *J. Mater. Chem.*, 2012, **22**, 20857.
20 Z. Jian, L. Zhao, H. Pan, Y-S. Hu, H. Li, W. Chen and L. Chen, *Electrochem. Commun.*, 2012, **14**, 86.
21 K. Saravanan , C. W. Mason , A. Rudola , K. H. Wong and P.Balaya, *Adv. Energy Mater.,* 2013, ***3***, 444.
22 Z. Jian , C. Yuan , W. Han , X. Lu , L. Gu , X. Xi , Y.-S. Hu , H. Li , W. Chen , D. Chen , Y. Ikuhara and L. Chen, *Adv. Funct. Mater.* 2014, **24**, 4265.
23 C. Zhu, K. Song, P. A. v. Aken, J. Maier and Y. Yu, *Nano Lett.* 2014, **14**, 2175.
24 N. Böckenfeld and A. Balducci, *J. Solid State Electrochem.*, 2014, **18**, 959.
25 W. Shen, C. Wang, H. Liu and W. Yang, *Chem. Eur. J.*, 2013, **19**, 14712.
26 Y. Uebou, T. Kiyabu, S. Okada and J.-i. Yamaki, *Rep. Inst. Adv. Mater. Study*, 2002, **16**, 1.
27 W. Song, X. Ji, Y. Yao, H. Zhu, Q. Chen, Q. Sun and C. E. Banks, *Phys. Chem. Chem. Phys.*, 2014, **16**, 3055.
28 W. Song, X. Ji, Z. Wu, Y. Zhu, Y. Yang, J. Chen, M. Jing, F. Li and C. E. Banks, *J. Mater. Chem. A*, 2014, **2**, 5358.
29 H. Y-P. Hong, *Mat. Res. Bull.*, 1976, **11**, 173.
30 W. Song, X. Ji, Z. Wu, Y. Zhu, F. Li, Y. Yao and C. E. Banks, *RSC Adv.*, 2014, **4**, 11375.
31 S. Y. Lim, H. Kim, R. A. Shakoor, Y. Jung and J. W. Choi, *J. Electrochem. Soc.*, 2012, **159**, 1393.
32 Y. Noguchi, E. Kobayashi, L. S. Plashnitsa, S. Okada and J.-i. Yamaki, *Electrochim. Acta*, 2013, **101**, 59.
33 F. Lalère, J.B. Leriche, M. Courty, S. Boulineau, V. Viallet, C. Masquelier and V. Seznec, *J. Power Sources*, 2014, **247**, 975.
34 B. Ellis, L. K. Perry, D. H. Ryan and L. F. Nazar, *J. Am. Chem. Soc.*, 2006, **128**, 11416.
35 T. Maxisch, F. Zhou and G. Ceder, *Phys. Rev. B*, 2006, **73**, 104301.
36 S. P. Ong, V. L. Chevrier and G. Ceder, *Phys. Rev. B*, 2011, **83** 075112.
37 V. A. Dinh, J. Nara and T. Ohno, *Appl. Phys. Express*, 2012, **5**, 045801.
38 K. M. Bui, V. A. Dinh and T. Ohno, *Appl. Phys. Express*, 2012, **5**, 125802.
39 K. M. Bui, V. A. Dinh and T. Ohno, *J. Phys: Conf. Ser.*, 2013, **454**, 012061.
40 K. M. Bui, *Two redox potentials cathode material Li_2MSiO_4 (M = Fe, Mn and Ni) for rechargeable Li batteries: A first principles study*, University of Tsukuba 2013.
41 D. M. Duong, V. A. Dinh and T. Ohno, *Appl. Phys. Express*, 2013, **6**, 115801.
42 J. Heyd, G. E. Scuseria and M. Ernzerhof, *J. Chem. Phys.*, 2003, **118**, 8207.
43 J. Perdew, K. Burke and M. Ernzerhof, *Phys. Rev. Lett.*, 1996, **77**, 3865.
44 G. Henkelman and H. J. Jonsson, *Chem. Phys.*, 2000, **113**, 9978.
45 G. Kresse and J. Hafner, *Phys. Rev. B.*, 1993, **47,** 558.
46 I.A. Courtney, J.S. Tse, O. Mao, J. Hafner and J.R. Dahn, *Phys. Rev. B*, 1998, **58** 15583.

